Article No. jmbi.1999.3435 available online at http://www.idealibrary.com on IDEAL® J. Mol. Biol. (2000) 296, 449–457

JMB

Direct Visualisation of Conformational Changes in EF_0F_1 by Electron Microscopy

Bettina Böttcher*, Ingo Bertsche, Rolf Reuter and Peter Gräber

Institut für Physikalische Chemie, Universität Freiburg Albertstraße 23a D-79104, Freiburg Germany

*Corresponding author

The isolated H^+-ATPase from *Escherichia coli* (EF_0F_1) was investigated by electron microscopy of samples of negatively stained monodisperse molecules, followed by single-particle image processing. The resulting three-dimensional maps showed that the F_1-part is connected by a prominent stalk to a more peripheral part of F_0. The F_1-part showed stain-accessible cavities inside. In three-dimensional maps from selected particles, a second stalk could be detected which was thinner than the main stalk and is thought to correspond to the stator.

Three-dimensional maps of the enzyme in the absence and in the presence of the substrate analogue adenyl-β,γ-imidodiphosphate (AMP-PNP) were calculated. Upon binding of AMP-PNP the three-dimensional maps showed no significant changes in the F_0-part of EF_0F_1, whereas a major conformational change in the F_1-part was observed. (1) The diameter of the F_1-part decreased upon binding of AMP-PNP mainly in the upper half of F_1. (2) Enzyme particles prepared in the presence of AMP-PNP had a pointed cap at the top of the F_1-part which was missing in its absence. (3) The stain-accessible cavity inside the F_1-part altered its pattern significantly.

Keywords: conformational change; electron microscopy; H^+-ATPase; image processing; 3D-map

Introduction

Membrane-bound H^+-ATPases of the F_0F_1-type catalyse ATP synthesis and ATP hydroysis coupled with a transmembrane proton transport in bacteria, chloroplasts and mitochondria (Mitchell, 1966). The H^+-ATPases have two large domains, a membrane-integrated F_0-part, which is involved in proton transport, and a hydrophilic F_1-part, which carries the nucleotide binding sites. In *Escherichia coli* the F_1-part consists of five different subunits with the stoichiometry $(\alpha\beta)_3\gamma\delta\varepsilon$, and the F_0-part consists of three different subunits with the likely stoichiometry $ab_2c_{9\text{-}12}$. Based on functional studies it is suggested that the three catalytic nucleotide binding sites of the β-subunits undergo conformational changes, adopting in sequential order the open, tight and loose conformation. This should be accomplished by subsequent ''docking-undocking'' steps of the γ-subunit to the three αβ-pairs, i.e. by rotation of the γ-subunit. The binding change model of ATP synthesis proposes a functional cooperation of the catalytic sites in a cyclic movement (for reviews, see Boyer, 1997; Cross, 1981).

For the isolated F_1 it was shown that during ATP hydrolysis the central γ-subunit rotates with respect to the α and β-subunits (Duncan *et al.*, 1995; Sabbert *et al.*, 1996, 1997; Noji *et al.*, 1997). Presumably, the ε-subunit rotates together with the γ-subunit. This was concluded from the finding that cross-linking of ε and γ-subunits had no influence on Mg^{2+}-ATPase activity (Schulenberg *et al.*, 1997), and this view is supported by the results of other cross-link experiments, confirming that the γ and ε-subunits are essentially randomly distributed between the α-subunits (Aggeler *et al.*, 1997). The structural and functional data were combined into a tentative model of the enzyme complex with its rotating portion (''rotor'') formed by the γ and the ε-subunit and the membrane-embedded ring of 12 copies of subunit c. The subunits b_2, δ and $(\alpha\beta)_3$ were assigned to the static part (''stator'') (Engelbrecht & Junge, 1997). A quantitative model under which such an assembly can generate the

Present address: B. Böttcher, EMBL-Heidelberg, Meyerhofstrasse 1, Postfach 102209, D-69012 Heidelberg, Germany.

Abbreviations used: AMP-PNP, adenyl-β,γ-imidodiphosphate.

E-mail address of the corresponding author: bottcher@embl-heidelberg.de

0022-2836/00/020449–9 $35.00/0

required power for ATP synthesis is described by Elston *et al*. (1998). The rotor-stator concept requires two stalks connecting F_1 to F_0. One of the two stalks belongs to the rotor and is built of the subunits γ and ε. The other stalk belongs to the stator and might consist of the subunits b_2 and δ. Two-dimensional projection maps of negatively stained H^+-ATPases from chloroplasts (Böttcher *et al*., 1998), *E. coli* (Wilkens & Capaldi, 1998) and mitochondria (Karrasch & Walker, 1999) indicated the existence of a second stalk.

There are atomic models for several subunits forming the H^+-ATPase. The structure of large regions of the mitochondrial F_1-part in the presence of adenyl-β,γ-imidodiphosphate (AMP-PNP) was determined from X-ray analysis to near atomic resolution (Abrahams *et al*., 1994). From NMR measurements atomic models of the isolated δ (Wilkens *et al*., 1997), ε (Wilkens *et al*., 1995) and the membrane integrated part of the b-subunit (Dimitriev *et al*., 1999) and c-subunits (Girvin *et al*., 1998) were established. However, there is only little structural information on the connection between the F_0-part and the F_1-part, i.e. on the part that is essential for the coupling of proton transport and ATP-synthesis/hydrolysis in the F_0F_1 complex. A suitable approach to investigate conformational changes occurring during the reaction cycle of H^+-ATPases might be time-resolved electron cryo-microscopy of single molecules. Small asymmetric particles like the EF_0F_1 complex are currently at the lower size limit for accurate determination of particle orientations (Henderson, 1995), and therefore it is difficult to calculate reliable three-dimensional maps of the H^+-ATPase embedded in vitrified water. We decided to find out whether it is possible to determine particle orientations of EF_0F_1 working with negatively stained samples. The data analysis showed that there was sufficient information to calculate three-dimensional maps of EF_0F_1. In addition we could detect remarkable conformational changes in the F_1-part upon binding of AMP-PNP, whereas the F_0-part stayed unaltered at this level of resolution.

Results

Electron micrographs of negatively stained EF_0F_1 protein molecules prepared in the presence or absence of AMP-PNP showed a mono-disperse distribution of particles (Figure 1). The intact enzyme complexes had two structurally distinct domains with a gap between. One part appeared to be slightly larger than the other. The overall shape can be described as dumbbell-like. The larger part most likely corresponds to the F_1-part and the smaller part to the F_0-part. To ensure that the selected particles are intact EF_0F_1 molecules, only those particles were chosen for image processing, whose structural domains were discernible.

About 5000 particles each were collected from samples prepared either in the presence or absence of AMP-PNP and processed independently. The resulting class averages of the particles prepared in a medium free of AMP-PNP or in the presence of AMP-PNP showed two distinct domains, a larger, more spherical domain corresponding to the F_1-part and a slightly smaller domain corresponding to the F_0-part. On average, the diameter of the larger domain was increased by about 15% in the absence of AMP-PNP. No significant changes were detected in the smaller domain. The two domains were connected by one or two stalks.

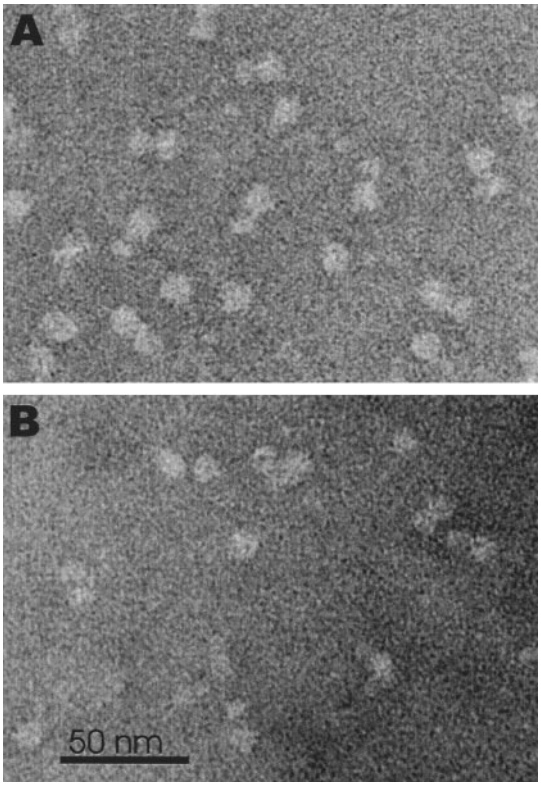

Figure 1. Electron micrograph of negatively stained EF_0F_1. Protein is bright against a darker background. (a) EF_0F_1 particles in the absence of AMP-PNP. (b) EF_0F_1 particles in the presence of 10 mM AMP-PNP.

The spatial relation between the class averages was determined using sinograms (Van Heel, 1987). The class averages were combined into independent three-dimensional maps of F_0F_1 complexes free of AMP-PNP and those with bound AMP-PNP. Surface presentations and central slices of the resulting maps are shown in Figure 2. In the surface representation (Figure 2(a) and (b)) the smaller domain, which corresponds to the F_0-part, had virtually the same appearance in both maps. It was slightly tapered at one end and showed little modulation on the inside. The wider end was connected to a massive stalk which formed a connection to the base of the larger domain corresponding to the F_1-part. The F_1-part was more spherical and differed in both maps. In the preparations with AMP-PNP it had a cap-like pointed

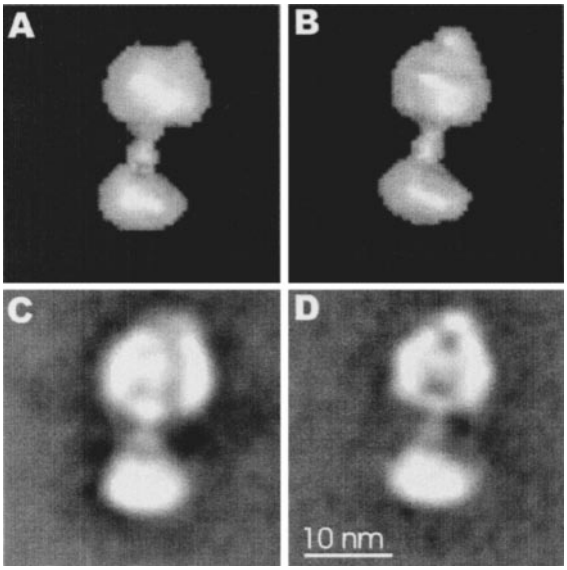

Figure 2. Surface representations and central slices through the three-dimensional maps of EF_0F_1 in the presence and absence of AMP-PNP. Protein density is shown bright against a darker background. (a) and (b) Surface presentations of the map (a) in the absence and (b) in the presence of AMP-PNP. (c) and (d) Central slices (thickness 0.56 nm) of the three-dimensional maps (c) in the absence and (d) in the presence of AMP-PNP.

region at the top of the F_1-part (Figure 2(b), which was missing in the absence of AMP-PNP (Figure 2(a)). Instead, a small spike could be found which was located at one side of the F_1-part. The diameter of the F_1-part parallel with the plane of membrane was significantly increased in the particles prepared without AMP-PNP. The central sections through the map (Figure 2(c) and (d)) showed a stain-accessible cavity on the inside of the F_1-part. The form of the cavity was clearly different in the presence and absence of AMP-PNP. With AMP-PNP bound, the cavity consisted of two areas of low density, one in the upper central region of F_1 and one in the lower central region of the F_1-part. In the samples prepared without AMP-PNP, the areas of low density in the upper and lower central region of the F_1-part had disappeared, and areas of low density on either side of a central rod emerged which were missing in the maps obtained after incubation of EF_0F_1 with AMP-PNP.

Different sections of the maps of the EF_0F_1 particles with and without bound AMP-PNP and the difference map of each pair of sections are shown in Figure 3. The maps were aligned with respect to their F_0-parts. The sections run approximately perpendicular to the supposed plane of the membrane. They were nearly 0.6 nm thick and were spaced by about 1.7 nm. The F_1-part extended from the first section to a section at a distance of 11.8 nm. The F_0-part extended from the first section to a section at a distance of 10.1 nm. In the difference map additional densities of the enzyme free of AMP-PNP are dark and additional densities of the particles with bound AMP-PNP are bright against a generally grey background. Only minor differences in the F_0-part occurred, which indicated that the observed differences could not be attributed to a mismatch in magnification of the initial micrographs. The main changes were all located in the F_1-part. A dark fringe surrounded most of the F_1-part, which implies that the diameter of the particle free of AMP-PNP is larger than that of the particle with bound AMP-PNP. Most of these differences appeared to be located in the upper half of the F_1-part. In a central section at a distance

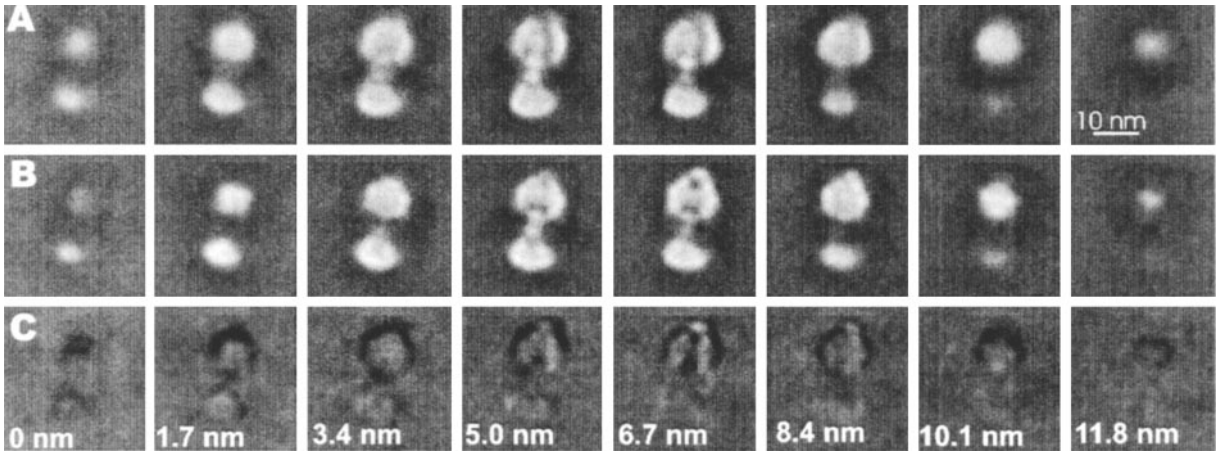

Figure 3. Sections of the three-dimensional maps of EF_0F_1 in the presence and absence of AMP-PNP and their difference. The slices are 0.56 nm thick and spaced by 1.68 nm. They are running perpendicular to the supposed plane of membrane. The distance of each individual slice from the first slice is indicated at the bottom. Density is shown bright against a general grey background. (a) Slices through the three-dimensional map of EF_0F_1 in the absence of AMP-PNP. (b) Slices through the three-dimensional map of EF_0F_1 in presence of AMP-PNP. The difference map, (b)−(a), is shown in (c). The difference map is shown at the same grey value distribution as the original maps.

of 6.7 nm from the first section, a strong pattern of two dark areas in the centre was surrounded by brighter areas, indicating that the stain-accessible cavity in the centre of the F_1-part had changed after binding of AMP-PNP.

In recent electron microscopic investigations (Wilkens & Capaldi, 1998; Karrasch & Walker, 1999; Böttcher *et al*., 1998) two-dimensional projection averages were calculated and showed that two stalks connect F_1 and F_0. The three-dimensional maps we have discussed so far resolve only one prominent stalk. A second stalk can barely be seen in Figure 2(d). With AMP-PNP bound to the enzyme, the class averages frequently showed projections of the enzyme with two stalks. We selected those class averages on which the two connections were clearly visible in order to find the second stalk in a three-dimensional map. From these class averages (approximately 25 % of all particles) the spatial relations between the class averages were determined and a three-dimensional map was calculated. Different representations of this map are shown in Figure 4. The direction of view is the same for all three presentations. The three-dimensional map was almost identical with the three-dimensional map calculated from all class averages for the enzyme with AMP-PNP bound, as shown in Figures 2 and 3, but now two stalks connecting the F_1-part and F_0-part were evident. One of the two stalks was quite massive and connected the central part of F_1 to a more peripheral part of F_0. The density of the second stalk was weaker and could be visualised only by lowering the threshold level for the protein density in the surface presentation (Figure 4(c)). This second stalk was thinner and connected a peripheral part of F_1 to a peripheral part of F_0 opposite the larger stalk.

Figure 5 shows different sections of the map calculated from the selected class averages. The plane of these sections was approximately perpendicular to the two stalks. The sections were 0.6 nm thick and were spaced by 2.8 nm. They start at the crest

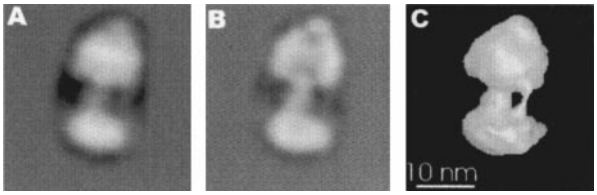

Figure 4. Different presentations of a three-dimensional map from selected class averages of EF_0F_1 in the presence of AMP-PNP. All three presentations show the same direction of view. Protein is shown bright against a darker background. The orientation is such that the upper domain corresponds to F_1 and the lower domain to F_0. (a) A projection map through all density. (b) A central slice (0.56 nm thick) through the density and (c) a surface presentation. A lower threshold for the density level for inclusion in the presented volume is chosen as in Figure 2 in order to display both connections between F_1 and F_0-parts.

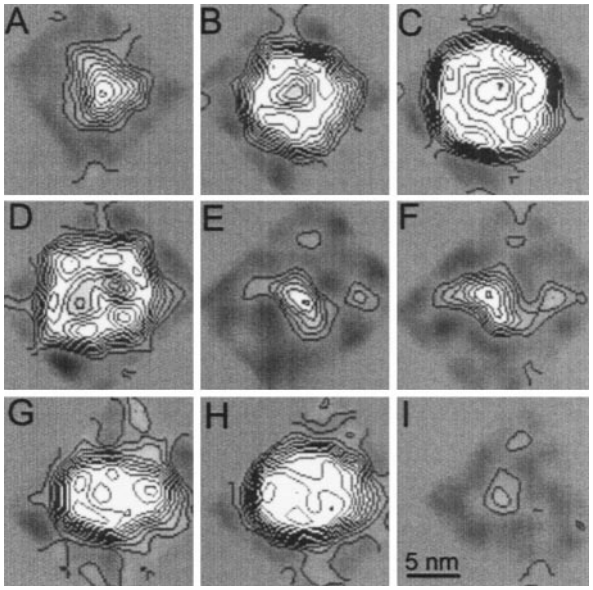

Figure 5. Slices through the three-dimensional map of selected class averages of EF_0F_1 in the presence of AMP-PNP. The slices are approximately perpendicular to the two stalks which are visible in Figure 4(c). The slices are 0.56 nm thick and spaced by 2.8 nm. Slices (a)-(d) correspond to the F_1-part. Slices (e) and (f) show the stalk region and the remaining three slices correspond to the F_0-part.

of the F_1-part, the first section cutting the cap-like structure at the top of F_1, which had a triangular cross-section. The F_1-part extended through four slices (Figure 5(a)-(d)). At the bottom part of F_1 is a ring-like structure formed by six centres of higher density with a hole in the middle. The stalk region extended through the next two slices (Figure 5(e) and (f)). In the stalk region there was a pattern of high density in the centre which corresponded to the prominent stalk (Figure 4(c)). In addition there were two areas of lower density which were much smaller. One was slightly stronger and a bit larger and corresponded to the second peripheral thinner stalk visible in Figure 4(c). Surprisingly, there was a third thin connection which was invisible in the class averages and in the surface presentations. This spot of density could perhaps correspond to a third connection between F_1 and F_0. The third and second stalk could be followed up to two protrusions at the outside of the base of the F_1-part (Figure 5(d)). The remaining three slices could be attributed to the F_0-part (Figure 5(g)-(i)). The F_0-part had an elongated cross-section. The upper region of F_0 was partly formed by a ring surrounding an area of low density. This area was located just underneath the centre of the massive central stalk. At one side of the ring-like structure an additional area of higher density could be observed. The two areas of lower density seen in the stalk region were connected to the periphery of this additional structure. These data indicated that there could actually be three stalks connecting the

F_1 and F_0-parts. The three stalks formed the corners of a triangle with the centre distances of 6-7 nm. This is well above the resolution of 1/3.5 nm^{-1} of the three-dimensional reconstructions. Therefore, the three stalks were clearly separated and could be detected as individual features. The diameter of the asymmetrically shaped central stalk was 4 nm by 7 nm. The diameter of the second and third stalk was smaller than the limit of resolution and therefore could not be determined accurately. It was estimated to be less than 2 nm.

The atomic model of the mitochondrial F_1-part (Abrahams *et al.*, 1994) was superimposed on the equivalent part of our three-dimensional map of EF_0F_1 in the presence of AMP-PNP (Figure 6(a)). The atomic model and our three-dimensional map fitted well in size and shape and even the stain-accessible cavities seen in our map could be assigned to cavities in the atomic model. Our 3D map showed additional density in the cap region of the F_1-part, which is missing in the atomic-model. The atomic model of the nucleotide-free $(\alpha\beta)_3$ complex of PS3 (Shirakihara *et al.*, 1997) was superimposed on our three-dimensional map of EF_0F_1 in the absence of AMP-PNP (Figure 6(b)). At the base of the F_1-part the atomic model and our three-dimensional map had about the same size. In the upper part of F_1 the fit between both models was unsatisfactory with our map showing a larger diameter and a different shape than the atomic model.

Discussion

The three-dimensional map computed from selected class averages of EF_0F_1 particles prepared in the presence of AMP-PNP (Figures 4 and 5) showed two connections between the F_1 and F_0-part as required by the rotor-stator model (Engelbrecht & Junge, 1997). Electron microscopic investigations of H^+-ATPase from *E. coli* (Wilkens & Capaldi, 1998), from chloroplasts (Böttcher *et al.* 1998) and from mitochondria (Karrasch & Walker, 1999) indicated the existence of two connections. All these investigations were carried out on negatively stained samples and showed two-dimensional projection maps of the H^+-ATPase, using preferential orientation of the sample on the carbon film (Karrasch & Walker, 1999), selection of favourable particles (Wilkens & Capaldi, 1998) or application of classification techniques (Böttcher *et al.*, 1998). However, on the basis of these data it is not possible to understand the spatial relation between the F_1-part and the F_0-part, and their interaction cannot be revealed in great detail. This can only be achieved when particle projections in different directions are combined into a three-dimensional map. For calculation of such a map of EF_0F_1, we assumed that the class averages from image analysis corresponded to different projections, and worked out their spatial relations using sinograms (Van Heel, 1987). The resulting three-dimensional maps showed an asymmetric particle. In the plane

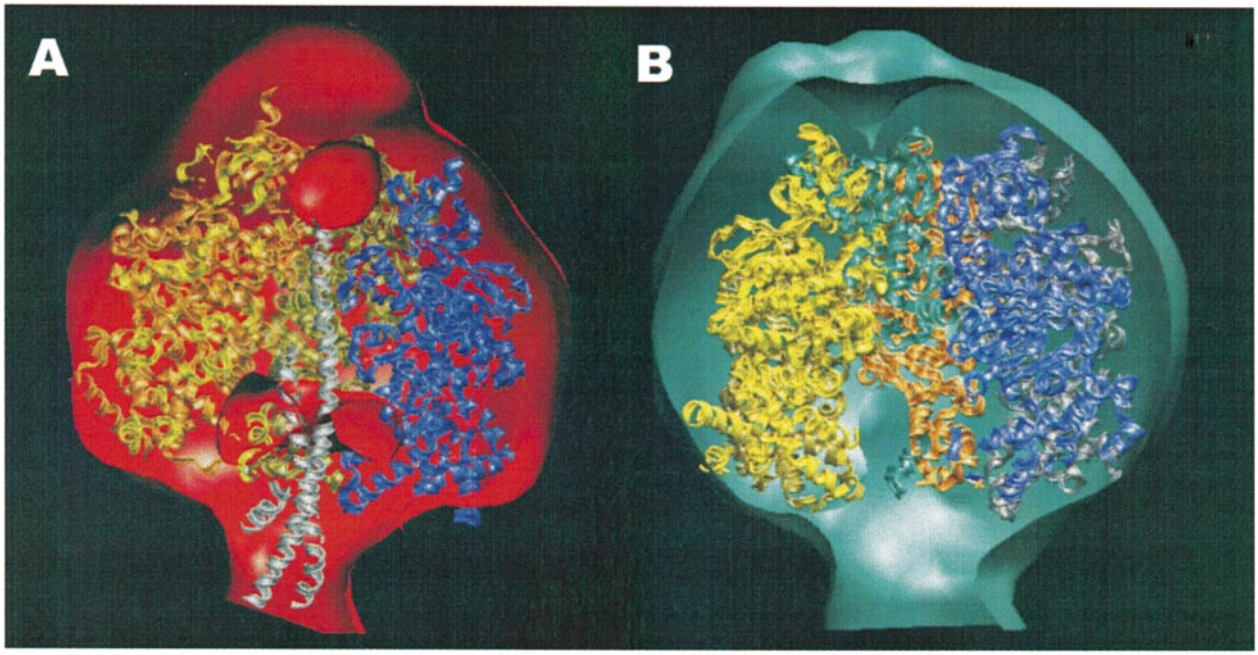

Figure 6. Superposition of electron microscopic three-dimensional maps and atomic models from X-ray analysis. (a) The F_1-part of the three-dimensional map of EF_0F_1 in the presence of AMP-PNP superimposed on the atomic model of MF_1 (Abrahams *et al.*, 1994). (b) The F_1-part of the three-dimensional map of EF_0F_1 in the absence of AMP-PNP superimposed on the atomic model of the $(\alpha\beta)_3$-complex of PS3 (Shirakihara *et al.*, 1997). The stain-accessible cavities are clearly seen in (a), top and bottom.

of the membrane the F_0-part is slightly elongated in one direction. The upper estimation for the diameter is 13 to 14 nm, whereas the smallest estimation for the diameter is about 10 nm. Since F_0 is surrounded by a micellar arrangement of detergent molecules, these values probably overestimate the true size of F_0 by up to 4-5 nm (Boekema *et al*., 1988).

The current model for F_0 proposes a ring-like complex of 9-12 copies of subunit c, with the a and b-subunits attached at the outside of the ring at one end (Engelbrecht & Junge, 1997). This would result in an elongated shape of F_0 in the plane of the membrane, as observed in our maps. A region of the F_0 in our three-dimensional maps has a greater membrane-spanning width and shows a slightly lower density on the inside. This part could correspond to the c-complex. The remaining part of F_0 has a smaller membrane-spanning width and is connected through one or two small stalks to the F_1-part. This portion could be formed by the membrane-integrated parts of the a and b-subunits.

Model calculations for the c-complex show a ring of nine to 12 subunits which are arranged around a central hole of an estimated diameter of roughly 3 nm (Groth & Walker, 1997). Such a hole would be large enough to allow small molecules to cross the membrane. It is clear that the hole has to be blocked in some way to prevent unrestricted passage of smaller molecules. A pore as large as postulated should be stain-accessible and therefore easy to detect in a three-dimensional map of a negatively stained protein. The only indication we could find for such a pore in the F_0-part was a slightly inhomogeneous distribution of density in that area (see e.g. Figure 3(b) and (c), third and fourth slice). This can be explained by a cavity which opens towards the F_1-part, but is partly closed by the stalk, and is completely closed towards the other side of F_0.

The stalk had an oval cross-section and was built of two distinct parts (Figures 2 and 3), one closer to the base of F_1, the other part closing the cavity in the F_0 moiety. It is widely agreed that the stalk is formed by the subunits ε and γ (Watts *et al*., 1996; Engelbrecht & Junge, 1997). Since γ and ε are supposed to transmit conformational changes caused by proton transport in the F_0-part to the nucleotide binding sites in the F_1-part, a rigid contact would be expected. Yet the stain-accessible interface indicates some flexible linkage.

The second connection between F_0 and F_1, which probably forms the stator, can only be detected under favourable conditions. Although some indication for the second connection can already be seen in the three-dimensional map deriving from the complete data set shown in Figures 2(d) and 3(b), this connection becomes much more visible if only class averages, which showed a clear indication for two connections between the F_0-part and the F_1-part, were included in the final 3D map (Figures 4 and 5). This selection might simply help choosing better preserved fully stain-embedded particles and therefore be more favourable for mapping the stator. It is assumed that the stator is partly formed by subunits b. Since there are two of these subunits per EF_0F_1 complex, one possibility would be that the second stalk consists of two of these subunits. There is an indication for a third connecting element between the F_1 and F_0-parts in the three-dimensional map obtained from selected class averages (Figure 5(e) and (f)). One possible explanation for the observation of the third connection might be the inclusion of some class averages with the wrong orientation in the final three-dimensional map. This is understandable, since the F_1-part has some pseudo-6-fold symmetry and therefore might easily cause rotational misalignment by multiples of 60°. However, the second and third connecting element are related by about 80° in respect to the pseudo-6-fold axis and therefore do not match this symmetry. In addition the F_0-part does not show a pseudo-6-fold symmetry at all, which makes such a misalignment unlikely. So the third connection could be a genuine property of EF_0F_1. This interpretation is encouraged by the recent discovery of three connecting stalks between V_0 and V_1 in V-type ATPase (Boekema *et al*., 1999). The position of the second and third connection in our map encourages another variation of structural arrangement for the stator elements in which the second and third connection are formed each by a single b-subunit. In this arrangement the b-subunits form a dimer contact in the upper F_1 region (Rodgers *et al*., 1997) and at the periplasmic side of the membrane (Dimitriev *et al*., 1999) but are well separated in the stalk region. This is supported by the NMR structure showing that the membrane-integrated part of the b-subunit is built by an α-helix which is kinked (Dimitriev *et al*., 1999). This kink could cause a separation of the two b-subunits in the stalk region. Another observation showed that EF_0F_1 is still functional after deletion of up to 11 amino acid residues (Sorgen *et al*., 1998). This supports the idea that there is some structural flexibility in the connection between the F_1-part and the F_0-part. According to secondary structure predictions, in the stalk region the b-subunits might be formed by a single α-helix. Such a small structural detail can only be detected under exceptionally favourable circumstances in negatively stained samples at this level of resolution. It is almost more surprising to detect these kind of details at all than missing them out.

EF_0F_1 shows remarkably big conformational changes upon binding of AMP-PNP. These changes were all located in the F_1-part. They can be summarised as a rearrangement in the cap-like region at the top of the F_1-part, a change in the stain-accessible cavity inside F_1 and a major decrease in the diameter of the F_1-part. All these changes could be observed in different maps calculated on the basis of different subsets of class averages. They were also observed when a three-dimensional map of the

EF_0F_1 complex prepared in the presence of AMP-PNP was used as the reference to determine the orientation of class averages of the particles free of AMP-PMP. Therefore, these changes are genuine conformational changes induced by binding of AMP-PNP to the F_1-part and were not caused by the variability in the maps.

The most striking change was the decrease in the diameter of F_1 upon binding of AMP-PNP. It can be ruled out that this was an artefact of slightly different magnification of the data-sets. When the enzymes were pre-treated with AMP-PNP in such a way that the ATP analogue was bound to only about 10% of the EF_0F_1 complexes, particles with large and small F_1 moieties could be detected by multivariate statistical analysis on the same micrograph (data not shown). The change in diameter observed here is consistent with a change of diffusion coefficients of EF_1 upon binding of AMP-PNP observed by single molecule fluorescence spectroscopy (Börsch *et al.*, 1998). There are also some indications from FTIR measurements that F_1 has an increased compactness and thermal stability if nucleotides are bound (Lippe *et al.*, 1995; Cladera *et al.*, 1995). Comparison between an atomic model of the nucleotide-free $(\alpha\beta)_3$ complex of the bacterium PS3 (Shirakihara *et al.*, 1997) and the atomic model of the bovine mitochondrial F_1-ATPase in presence of AMP-PNP (Abrahams *et al.*, 1994) also indicates some change in the diameter of the F_1-part. However, this structural difference is mainly caused by some hinge-like movements of the lower region of two of the three β-subunits and is much smaller than the change which we observe upon binding of AMP-PNP to the EF_0F_1-ATPase. In the maps presented here the main alteration in diameter is located in the upper half of F_1, as indicated by the difference map shown in Figure 3(c). Therefore, it cannot be solely explained by opening or closing of the nucleotide binding sites by a hinge-like movement of the lower part of the β-subunits, but such movement could account for the observed change in the stain-accessible cavity inside F_1. It should be pointed out that in the X-ray analysis only sub-complexes of the isolated F_1-part either from PS3 or from mitochondria were investigated, whereas our maps show the whole complex including the membrane-embedded F_0-part of *Escherichia coli*. The very simple composition of the PS3 sub-complex without the γ-subunit might show only parts of the structural changes involved upon binding of AMP-PNP. It could well be that some of the differences seen in our maps upon binding of AMP-PNP are due to the presence of the F_0-part and are probably showing conformational changes which are involved in the coupling of proton-transport to ATP-synthesis/hydrolysis. The change in the cap region upon binding of AMP-PNP presumably refers to some rearrangement in the N-terminal domains of the α and β-subunits, indicating a more complex rearrangement of the α and β-subunits. Surprisingly this N-terminal region, although located at the top of F_1, far from the membrane-integrated F_0-part, seems to be involved in (1) binding of the F_1-part to the F_0-part, (2) proton permeability through the F_0-part, and (3) coupling of ATP-hydrolysis to proton transport (Maggio *et al.*, 1988; Hase *et al.*, 1996; Xu *et al.*, 1996; Lill *et al.*, 1996).

The superposition of the atomic model of MF_1 in the presence of AMP-PNP (Abrahams *et al.*, 1994) on our three-dimensional map of the EF_0F_1 in the presence of AMP-PNP (Figure 6(a)) fits well, in size and shape. The main difference is some additional density in the cap region at the top of the F_1-part in our three-dimensional map, which is missing in the atomic model. This mismatch is presumably due to the missing N termini of the α and β-subunits in the atomic model. The superposition of the atomic model of the nucleotide-free $(\alpha\beta)_3$ complex of PS3 (Shirakihara *et al.*, 1997) on our three-dimensional map of EF_0F_1 in the absence of AMP-PNP (Figure 6(b)) does not match in size or in shape. At the bottom of the F_1-part both models have about the same size; therefore, a hinge-like movement of the lower part of the β-subunits might have taken place upon release of nucleotides. Nevertheless, the mismatch in the upper part of F_1 cannot be explained by this model and has to be attributed to some major rearrangement of subunits.

We have shown that electron microscopy of negatively stained samples and three-dimensional image reconstruction is a powerful tool for understanding the structure of EF_0F_1 at a low resolution level. The three-dimensional maps give a more detailed insight into the construction of the molecule than two-dimensional projection maps alone. Using this approach we were able to show that upon binding of AMP-PNP the F_1-part in EF_0F_1 shrinks, the stain-accessible cavity on the inside of the F_1-part alters its shape and that a cap-like structure at the top of F_1 evolves whereas the F_0-part stays unaltered.

Materials and Methods

EF_0F_1 was prepared by an isolation procedure similar to that described by Fillingame & Foster (1986). The SDS-PAGE of the isolated EF_0F_1 showed bands corresponding to the subunits α, β, γ, δ, ε, a, b and c. The protein concentration was measured by the method described by Popov *et al.* (1975) using bovine serum albumin as a standard. The isolated EF_0F_1 contained 1.5 mol of ATP and 0.9 mol of ADP bound per mol of enzyme using a molecular mass of 550 kg mol^{-1}.

EF_0F_1 samples without bound AMP-PNP were obtained as follows. The enzyme solution (1 μM) was diluted by a factor of 50-200 with a buffer containing 80 mM KCl, 2% (w/v) sucrose, 10% (w/v) glycerol, 4 mM $MgCl_2$, 2 mM dithiothreitol, 0.1% (w/v) dodecylmaltoside and 40 mM 3-[*N*-morpholino]propanesulfonic acid (pH 7.5) and immediately applied to a glow-discharged carbon-coated copper grid. The solution was incubated on the grid for three minutes then washed twice with water and stained for two minutes with a 2% (w/v) uranyl acetate solution.

The preparation of the enzyme complex with bound AMP-PNP was carried out in two steps. First a 100 μM Mg-ATP solution was added to the EF_0F_1 solution (1 μM) to give a final concentration of 10 μM Mg-ATP. The solution was incubated for two minutes at 25 °C. In the second step 100 mM AMP-PNP solution was added to the enzyme solution to give a final concentration of 10 mM AMP-PNP. For staining this sample was diluted 1:10 with the same buffer as described above containing in addition 10 mM AMP-PNP and was applied to glow-discharged carbon-coated copper grids. The grids were washed twice with 10 mM AMP-PNP solution (pH 6.0) and stained for two minutes with 2 % uranyl acetate.

Micrographs of AMP-PNP-free samples and samples in the presence of AMP-PNP were taken on a Philips EM 400 operating at 100 kV at a nominal magnification of 55,000×. Care was taken to minimise pre-exposure by focusing and adjusting brightness on an adjacent area. Micrographs were recorded on Kodak SO-163 film and developed in full-strength Kodak D-19 developer at room temperature. The absolute magnification of the electron microscope was calibrated with negatively stained catalase crystals and was 50,600×. This value was used for all further calculations.

Micrographs of particles in the presence of AMP-PNP and of AMP-PNP-free samples were processed independently. Suitable micrographs were scanned with an EMIL-line scan camera (IMAGE SCIENCE, GmbH). The calibrated pixel size was 14.15 μm per pixel. Two-by-two pixels were combined to give a final pixel size of 0.56 nm by 0.56 nm at the specimen level. Image processing was carried out using the IMAGIC software package (Van Heel *et al*., 1996) and the MRC-image processing programs (Crowther *et al*., 1996). Particles showing two domains were selected, boxed and normalised in their grey value distribution and band-pass filtered to cut off spatial frequencies above $1/1.7\ nm^{-1}$ and below $1/22.4\ nm^{-1}$. Approximately 5000 particles from different micrographs were included in each set. The boxed particles were aligned to a common reference and classified into 200 classes (Borland & Van Heel, 1990; Van Heel, 1989). The spatial relations between classes were calculated using sinograms (Van Heel, 1987). The classes were then combined into three-dimensional maps. The three-dimensional maps were reprojected in the same directions as the orientations of the class averages. These reprojected images were used as new references for a multi-reference alignment of the data-set, followed by new classification and determination of the orientation of the class averages. The class averages were then combined into the current best map. The last four steps (alignment to projections of the current best map, classification, determination of orientations and calculation of a three-dimensional map) were repeated until no further improvement was observed. For difference imaging the three-dimensional maps were normalised in their grey value distribution and subtracted slice-by-slice. For estimation of resolution of each map two independent maps of half of the class averages were calculated and their Fourier shell correlation was calculated. In both maps the correlation drops to 0.5 at a spatial frequency of $1/3.6\ nm^{-1}$ and reaches 4σ at a spatial frequency of $1/2.7\ nm^{-1}$.

The atomic models were pre-docked to the electron microscopic three-dimensional map using the Situs-package 1.0 (Wriggers *et al*., 1999). The pre-docked atomic models were than manually adjusted using the VMD package. (Lill *et al*., 1996).

Acknowledgements

We thank Dietrich Samoray for critical reading of the manuscript. R. R. and I. B. acknowledge support of Graduiertenkolleg Biochemie der Enzyme. This work was supported by Deutsche Forschungsgemeinschaft (SFB 428) and (BO-1150/3).

References

Abrahams, J. P., Leslie, A. G., Lutter, R. & Walker, J. E. (1994). Structure at 2.8 Å resolution of F_1-ATPase from bovine heart mitochondria. *Nature,* **370**, 621-628.

Aggeler, R., Ogilvie, I. & Capaldi, R. A. (1997). Rotation of γ-ε subunit domain in the *Escherichia coli* F_1F_0-ATP synthase complex. The γ-ε subunits are essentially randomly distributed relative to the $\alpha_3\beta_3\delta$ domain in the intact complex. *J. Biol. Chem.* **272**, 19621-19624.

Boekema, E. J., Schmidt, G., Gräber, P. & Berden, J. A. (1988). Structure of the ATP-synthase from chloroplasts and mitochondria studied by electron microscopy. *Z. Naturforsch.* **43c**, 219-225.

Boekema, E. J., Van Breemen, J. F., Brisson, A., Ubbink-Kok, T., Konings, W. N. & Lolkema, J. S. (1999). Connecting stalks in V-type ATPase. *Nature,* **401**, 37-38.

Borland, L. & Van Heel, M. (1990). Classification of image data in conjugate representation spaces. *J. Opt. Soc. Am. ser. A,* **7**, 601-610.

Börsch, M., Turina, P., Eggeling, C., Fries, J. R., Seidel, C. A., Labahn, A. & Gräber, P. (1998). Conformational changes of the H^+-ATPase from *Escherichia coli* upon nucleotide binding detected by single molecule fluorescence. *FEBS Letters,* **437**, 251-254.

Böttcher, B., Schwarz, L. & Gräber, P. (1998). Direct indication for the existence of a double stalk in CF_0F_1. *J. Mol. Biol.* **281**, 757-762.

Boyer, P. D. (1997). The ATP synthase - a splendid molecular machine. *Annu. Rev. Biochem.* **66**, 717-749.

Cladera, J., Villaverde, J., Hartog, A. F., Padrós, E., Berden, J. A., Rigaud, J.-L. & Dunach, A. (1995). Influence of nucleotides on the secondary structure and on the thermal stability of mitochondrial F_1 visualized by infrared spectroscopy. *FEBS Letters,* **371**, 115-118.

Cross, R. L. (1981). The mechanism and regulation of ATP synthesis by F_1-ATPases. *Annu. Rev. Biochem.* **50**, 681-714.

Crowther, R. A., Henderson, R. & Smith, J. M. (1996). MRC image processing programs. *J. Struct. Biol.* **116**, 9-16.

Dimitriev, O., Jones, P. C., Weiping, J. & Fillingame, R. (1999). Structure of the membrane domain of subunit b of the *Escherichia coli* F_0F_1 ATP synthase. *J. Biol. Chem.* **274**, 15598-15604.

Duncan, T. M., Bulygin, V. V., Zhou, Y., Hutcheon, M. L. & Cross, R. L. (1995). Rotation of subunits during catalysis by *Escherichia coli* F_1-ATPase. *Proc. Natl Acad. Sci. USA,* **92**, 10964-10968.

Elston, T., Wang, H. & Oster, G. (1998). Energy transduction in ATP synthase. *Nature,* **391**, 510-513.

Engelbrecht, S. & Junge, W. (1997). ATP synthase: a tentative structural model. *FEBS Letters,* **414**, 485-491.

Fillingame, R. H. & Foster, D. L. (1986). Purification of F_0F_1 H^+-ATPase from *Escherichia coli*. *Methods Enzymol.* **126**, 545-557.

Girvin, M. E., Rastogi, V. K., Abildgaard, F., Markley, J. L. & Fillingame, R. H. (1998). Solution structure of the transmembrane H^+-transporting subunit c of the F_0F_1 ATP synthase. *Biochemistry*, **37**, 8817-8824.

Groth, G. & Walker, J. E. (1997). Models of the c-subunit oligomer in the membrane domain of F-ATPases. *FEBS Letters,* **410**, 117-123.

Hase, B., Werner-Grüne, S., Deckers-Hebestreit, G. & Strotmann, H. (1996). Site-directed mutagenisis of two conserved charged amino acids in the N-terminal region of the α-subunit of *E. coli*-F_0F_1. *FEBS Letters,* **382**, 171-174.

Henderson, R. (1995). The potential limitations of neutrons, electrons and X-rays for atomic resolution microscopy of unstained biological molecules. *Quart. Rev. Biophys.* **28**, 171-193.

Hermolin, J., Dimitriev, O. Y., Zhang, Y. & Fillingame, R. (1999). Defining the domain of binding of F_1 subunit ε with the polar loop of F_0 subunit c in the *Escherichia coli* ATP synthase. *J. Biol. Chem.* **274**, 17011-17016.

Karrasch, S. & Walker, J. E. (1999). Novel features in the structure of bovine ATP synthase. *J. Mol. Biol.* **290**, 379-384.

Lill, H., Hensel, F., Junge, W. & Engelbrecht, S. (1996). Cross-linking of engineered subunit δ to $(\alpha\beta)_3$ in chloroplast F-ATPase. *J. Biol. Chem.* **271**, 32737-32742.

Lippe, G., Di Pancrazio, F., Dabbeni-Sala, F., Bertoli, E. & Tanfani, F. (1995). Influence of ADP, AMP-PNP and a depletion of nucleotides on the structural properties of F_1-ATPase: a Fourier transform infrared spectroscopic study. *FEBS Letters,* **373**, 141-145.

Maggio, M. B., Parsonage, D. & Senior, A. E. (1988). A mutation in the α-subunit of F_1-ATPase from *Escherichia coli* affects the binding of F_1 to the membrane. *J. Biol. Chem.* **263**, 4619-4623.

Mitchell, P. (1966). Chemiosmotic coupling in oxidative and photosynthetic phosphorylation. *Biol. Rev. (Cambridge),* **41**, 445-502.

Noji, H., Yasuda, R., Yoshida, M. & Kinosita, K., Jr (1997). Direct observation of the rotation of F_1-ATPase. *Nature,* **386**, 299-302.

Popov, N., Schmidt, M., Schulzeck, S. & Matthies, H. (1975). Eine störungsfreie Mikromethode zur Bestimmung des Proteingehaltes in Gewebehomogenaten. *Acta Biol. Med. Germ.* **34**, 1441-1446.

Rodgers, A. J., Wilkens, S., Aggeler, R., Morris, M. B., Howitt, S. M. & Capaldi, R. A. (1997). The subunit delta-subunit b domain of the *Escherichia coli* F_1F_0 ATPase. The b subunits interact with F_1 as a dimer through the delta subunit. *J. Biol. Chem.* **272**, 31058-31064.

Sabbert, D., Engelbrecht, S. & Junge, W. (1996). Intersubunit rotation in active F-ATPase. *Nature,* **381**, 623-625.

Sabbert, D., Engelbrecht, S. & Junge, W. (1997). Functional and idling rotatory motion within F_1-ATPase. *Proc. Natl Acad. Sci. USA,* **94**, 4401-4405.

Schulenberg, B., Wellmer, F., Lill, H., Junge, W. & Engelbrecht, S. (1997). Cross-linking of chloroplast F_0F_1-ATPase subunit ε to γ without effect on activity. ε and γ are parts of the rotor. *Eur. J. Biochem.* **249**, 134-141.

Shirakihara, Y., Leslie, A. G., Abrahams, J. P., Walker, J. E., Ueda, T., Sekimoto, Y., Kambara, M., Saika, K., Kagawa, Y. & Yoshida, M. (1997). The crystal structure of the nucleotide-free α_3 β_3 subcomplex of F_1-ATPase from the thermophilic *Bacillus* PS3 is a symmetric trimer. *Structure,* **5**, 825-836.

Sorgen, P. L., Caviston, T. L., Perry, R. C. & Cain, B. D. (1998). Deletion in the second stalk of F_1F_0-ATP synthase in *Escherichia coli*. *J. Biol. Chem.* **273**, 27873-27878.

Van Heel, M. (1987). Angular reconstitution: a posteriori determination of projection directions for 3D reconstructions. *Ultramicroscopy,* **21**, 111-124.

Van Heel, M. (1989). Classification of very large electron microscopical image data sets. *Optik,* **82**, 114-126.

Van Heel, M., Harauz, G., Orlova, E. V., Schmidt, R. & Schatz, M. (1996). A new generation of the IMAGIC image processing system. *J. Struct. Biol.* **116**, 17-24.

Watts, S. D., Tang, C. & Capaldi, R. A. (1996). The stalk region of *Escherichia coli* ATP synthase. Tyrosine 205 of the γ subunit is in the interface between F_1 and F_0 parts and can interact with both the ε and c oligomer. *J. Biol. Chem.* **271**, 28341-28347.

Wilkens, S. & Capaldi, R. A. (1998). Electron microscopic evidence of two stalks linking the F_1 and F_0 parts of the *Escherichia coli* ATP synthase. *Biochim. Biophys. Acta,* **1365**, 93-97.

Wilkens, S., Dahlquist, F. W., McIntosh, L. P., Donaldson, L. W. & Capaldi, R. A. (1995). Structural features of the epsilon subunit of the *Escherichia coli* ATP synthase determined by NMR spectroscopy. *Nature Struct. Biol.* **2**, 961-967.

Wilkens, S., Dunn, S. D., Chandler, J., Dahlquist, F. W. & Capaldi, R. A. (1997). Solution structure of the N-terminal domain of the delta subunit of the *E. coli* ATPsynthase. *Nature Struct. Biol.* **4**, 198-201.

Wriggers, W., Milligan, R. A. & McCammon, J. A. (1999). Situs: a package for docking crystal structures into low resolution maps from electron microscopy. *J. Struct. Biol.* **125**, 185-195.

Xu, T., Candita, C. & Papa, S. (1996). The effect of mild trypsin digestion of F_1 on energy coupling in the mitochondrial ATP synthase. *FEBS Letters,* **397**, 308-312.

Edited by W. Baumeister

(Received 10 August 1999; received in revised form 30 November 1999; accepted 30 November 1999)